
Article:
Li, Y., Fan, F., Wang, J. et al. (4 more authors) (2019) New type of columnar liquid crystal superlattice in double-taper ionic minidendrons. Chemistry – A European Journal, 25 (60). pp. 13739-13747. ISSN 0947-6539

https://doi.org/10.1002/chem.201902639

New Type of Columnar Liquid Crystal Superlattice in Double-Taper Ionic Minidendrons

Ya-xin Li,[a,†] Fang-fang Fan,[b,†] Jie Wang,[b,c] Liliana Cseh,[c,d] Min Xue,[b] Xiang-bing Zeng[a] and Goran Ungar[c*]

[a] Department of Materials Science and Engineering, University of Sheffield, Sheffield S1 3JD, U.K.
[b] Department of Physics, Zhejiang Sci-Tech University, Hangzhou 310018, P.R. China
[c] State Key Laboratory for Mechanical Behavior of Materials, School of Materials, Xi'an Jiaotong University, Xi'an 710049, P.R. China
[d] "Coriolan Dragulescu" Institute of Chemistry, Timisoara 300223, Romania

Abstract

Wedge-shaped molecules, such as dendrons, are among the most important building blocks for directed supramolecular self-assembly. Here we present a new approach aimed at widening the range and complexity of potential mesophases by introducing *double-tapered* mesogens. Two series of compounds are presented, both alkali metal salts (Li, Na, Cs) of 3,4,5-*tris*-alkoxybenzoic acid with a second tapered *tris*-alkoxyaryl group attached at the end of an alkoxy chain. The double-tapered compounds all display an unusual hexagonal columnar phase consisting of one ionic and three non-ionic columns per unit cell. The cation size has an unexpectedly drastic effect on unit cell size. Unlike most columnars, the current phases show unusually high dimensional stability on heating, and high stiffness in spite of being 80-85% aliphatic, attributed to their molecular topology. The described approach may lead to co-assemblies of multifunctional materials, e.g. parallel *p*- and *n*-semiconducting nanowires or parallel ionic and electronic conductors.

Introduction

Columnar liquid crystal phases, having 2D positional order, have come a long way since their first discovery in 1977 in discotic molecules.[1] Subsequent years have seen columnar mesogens increasing in complexity and variety of shapes (star,[2,3] bent core,[4] bowl,[5,6] helicene,[7] heterocycle,[8] T- and X-shape[9]) and types of non-bonded interactions (H-bonding,[10] donor-acceptor[11], ionic,[12] coordination[13]).

Wedge-shaped molecules that consist of at least two moderately incompatible parts often exhibit liquid crystal (LC) phases with 2D or 3D periodicity. Typical compounds of this type are dendrons and "minidendrons" (first-generation wedge-shaped dendrons) containing an aromatic core and a functional group at the narrow end, and flexible terminal alkyl or oligo(ethylene oxide) chains at the wide end. The chains form a soft shell, or corona, that wrap around cylindrical columns or spherical "micelles".[14,15,16,17,18,19] Tapered mesogens, including dendrons, are some of the most fundamental and widespread building blocks in

† These authors contributed equally.

supramolecular chemistry. They have been included as assembly-directing moieties in functional materials such as organic semiconductors,[20,21] ionic conductors,[22,23,24,25,26] crown ethers,[27,28] donor-acceptor complexes,[29,30] polymers,[31,32,33] peptides,[34] nanoparticles[35,36] etc. In this way it is possible to create "dendronized" functional materials that can be used in a variety of potential applications.[37] Columnar organization, often due to the attachment of alkoxyphenyl dendrons,[14] can be usefully exploited, e.g. in forming 1D electronic[20,21] and ionic [22,23,24,25,26] conductors, in encapsulating drugs[38] and light-emitting polymers[39] etc.

The main factor determining whether columnar, spherical, layer-like or bicontinuous self-assembly mode is adopted by such molecules is the actual geometry of the wedge. In a first approximation the cross-section area of the wedge A increases as $A = k\,x^p$, where x is the distance from the narrow end see Figure 1a. For wedges forming cylindrical columns, $k = (2\pi/\mu)$, where μ is the number of wedges in the disk-like section (the "stratum") of the column. As a rough guide, smectic phases are favoured for $p \approx 0$ (no taper), hexagonal columnar for $p \approx 1$ ("pizza-slice"), spherical for $p \approx 2$ (parabolic wedge, or cone), and bicontinuous cubic for $0 < p < 1$ (shield-like) [40] – see Figure 1a. In a further crude approximation, small differences in the value of p close to 2 will determine the packing mode of spherical micelles, with the lowest p giving the Frank-Kasper A15 cubic phase, space-group $Pm\bar{3}n$ [41] and the highest p giving the body-centred cubic (BCC).[42] BCC seems to be the ultimate structure for wedges of highest divergence (highest p), as shown by benzoate salts with 5 chains emanating from a single phenyl ring. [43] In some cases for $0 < p < 1$ rectangular columnar, or "ribbon", phases form instead of bicontinuous cubic.[44,45,46] It has been shown that a temperature-induced transition between rectangular and hexagonal columnar phase in ionic LCs can be used as a thermal on-off switch for ionic conduction.[26]

Except for discotic molecules, the simplest and most common case of column-forming building blocks is that of a pointed wedge, e.g. a dendron tapered down to a small group at the apex, such as carboxylic acid, carboxylate salt, OH or $COOCH_3$.[14,47] Such tapered mesogens thus assemble like pizza-slices into a flat disk (Figure 1b), or if tilted, into a propeller- or umbrella-like object. The flexible chains form the liquid-like continuum outside the columns. The larger the taper angle, the smaller the μ (Figure 1c). There are also numerous examples of wedge-like molecules covalently connected together at their narrow end, forming dimers[48] (Figure 1d), as well as oligomers or polymers;[14] the polymer backbone then resides in the column centre. More unusual situations arise when the wedge is "blunt", as in the case of alkyl-substituted helicene in Figure 1e.[49] In that case a hole remains in the centre of the column, the column taking the shape of a helical tube. If the wedge is narrow and blunt, as in the case of biphenyl-based dendrons,[50] the number μ of molecules in a disk is large, but the blunt end means that the hole in the column centre also increases. As large voids are not tolerated in liquids or LCs, some molecules reverse their orientation plugging the central hole with their terminal chains (Figure 1f);[51] this results in an array of tightly packed vesicle-like aromatic cylinders, with flexible chains both inside and outside.

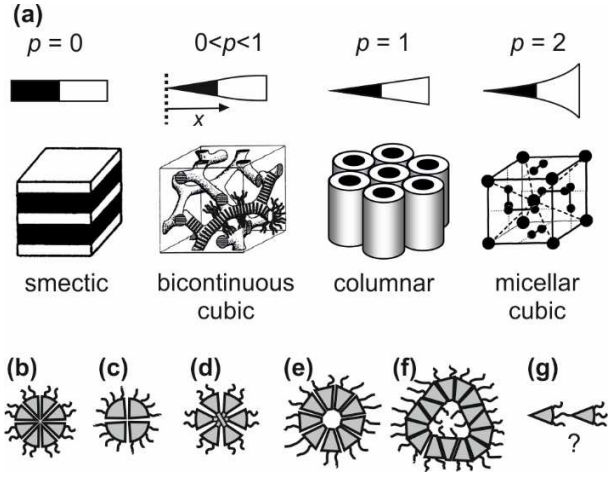

Figure 1. (a) Schematic representation of the effect of architecture of a wedge-shaped molecule on the type of their organization in a LC or soft crystal. (b-f) Different modes of arrangement of wedges in a cylindrical column (view along the column axis). (g) Double-tapered molecule.

The exact shape of the wedge can be tailored in a variety of ways, e.g. by changing the branching pattern at each successive generation cascade of a dendron, e.g. 3-way followed by 2-way branching - this often affects the nanostructure.[14] However, restricting the shape to a single wedge, regardless of its shape, still limits the variety of its modes of assembly. In this work we venture outside these limitations by designing molecules of a double wedge shape, where the periphery of the first, inner wedge is the starting point of a second, outer wedge – see (Figure 1g and Scheme 1). In this way we obtain a new columnar phase of complex superstructure comprising two different coexisting column types. A detailed structural study is presented, exploring the packing principles, morphology and stability of this new self-assembly mode with promising application potential.

Results

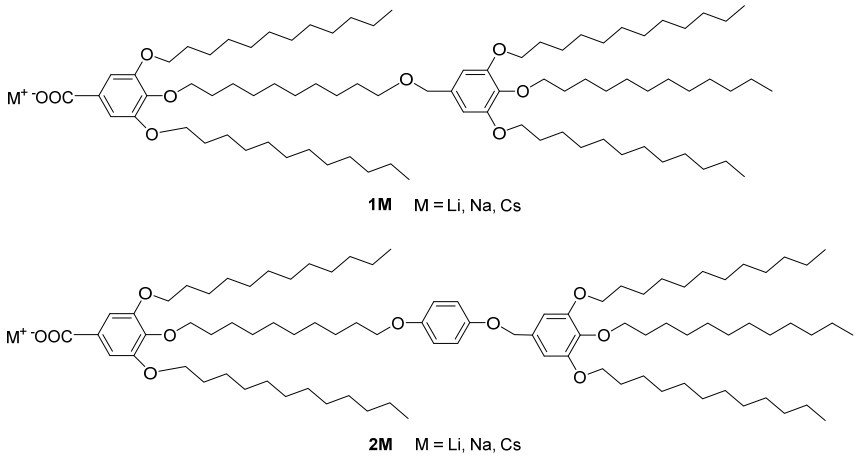

Scheme 1. Compounds **1M** and **2M**

Compounds **1M** and **2M** were prepared as described in Schemes S1 and S2 in SI. The inner tapered benzoate intermediate was synthesised by benzyl protection of the 4-position, alkylation of 3 and 5 positions and then selective

deprotection of the 4-position. The second tapered intermediates contained one (for compounds **1M**) or two (for **2M**) benzene rings and were obtained by etherification of methyl gallate with 1-bromododecane and subsequent ester group reduction in the presence of $LiAlH_4$ giving (3,4,5-tris(dodecyloxy)phenyl)methanol. To obtain **2M**, the preparation of the outer tapered intermediate for the synthesis of methyl3,5-bis(dodecyloxy)-4-((10-(4-((3,4,5-tris(dodecyloxy)benzyl) oxy)phenoxy)decyl)oxy)benzoate (**13**) involved two steps in addition to those for the preparation of methyl 3,5-bis(dodecyloxy)-4-((10-((3,4,5-tris(dodecyloxy)benzyl)oxy)decyl)oxy)benzoate (**9**), i.e. the conversion of hydroxyl group to halide and mono-etherification of 1,4-dihydroxybenzene with a bromo derivative. The inner and outer tapered mesogens were then linked by a *n*-dodecylene chain via two successive Williamson etherifications. The alkali metal salts were prepared by base-assisted hydrolysis of the methyl benzoate with the corresponding alkali metal hydroxides. As in other similar hygroscopic alkali metal salts, it is important to ensure that the material is free of water and that the carboxylic acid is fully ionized. Before analysis compounds **1M** and **2M** were dried *in vacuo* for 24 h at 40 °C. The IR spectra (Figure 2) confirm that the compounds were in order on both counts. The absence of water is shown by the absence of a broad O-H stretching peak in the range 3300-2500 cm^{-1} (but exposure to air produced a broad peak around 3300 cm^{-1}). Also, the spectra in Figure 2 contain a strong C=O stretching band at 1597 cm^{-1} due to carboxylate anion. Meanwhile C=O bands at 1687 cm^{-1} and 1720 cm^{-1} corresponding, respectively, to acid and ester (Figure S29), are completely absent, as is the free acid O-H bending vibration at 932 cm^{-1}.

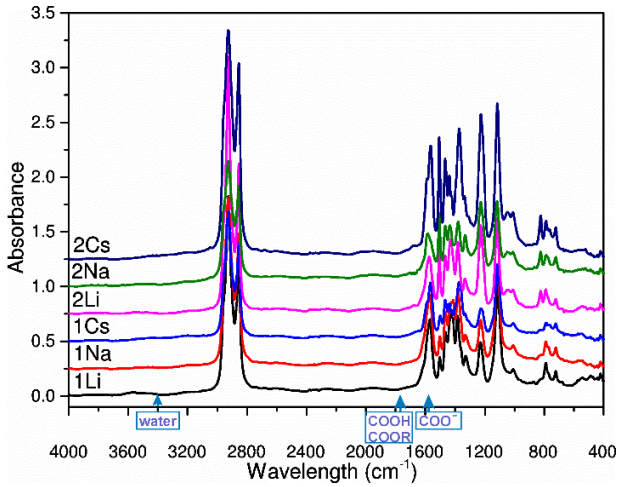

Figure 2. IR spectra of compounds **1M** and **2M** as films between CsI windows

The compounds were investigated by differential scanning calorimetry (DSC), polarized optical microscopy (POM) and X-ray scattering including powder small- and wide-angle (SAXS and WAXS), grazing incidence SAXS and WAXS (GISAXS and GIWAXS) on thin films, electron density map reconstruction and molecular modelling and molecular dynamics (MD) annealing.

Above a low crystal melting point, all compounds display a birefringent mesophase. The POM image in Figure 3a shows black regions, meaning that here the optic axis is perpendicular to the glass surface (homeotropic alignment)) and

therefore that the material itself is optically uniaxial. The circular or fan-like birefringent regions with a parts of a dark Maltese cross in Figure 3a suggest that these are the developable domains,[52] or "spherulitic" patterns, characteristic of columnar (Col) LC phases. The uniaxiality suggests that the mesophase is hexagonal. The image taken with the λ-plate (Figure 3b) shows that the high-index axis is radial in the developable domains, and since the columns are normally tangential, the high-index direction is perpendicular to the column axis. This is consistent with the columns being negatively birefringent, with the averaged orientation of the benzene rings normal to the column axis.

Figure 4 shows cooling DSC thermograms of all six compounds, with the isotropic (Iso) to columnar transition exotherm marked by arrow. The Iso-Col transition is highly reversible with low hysteresis as shown by heating thermograms, Table S1 in Supporting Information (SI). Transition temperatures and enthalpies are listed in Table 1. As can be seen, the isotropization transition temperature T_i decreases with increasing size of the metal cation, from Li to Cs, but is unaffected by the addition of the extra benzylether group in compounds **2M**.

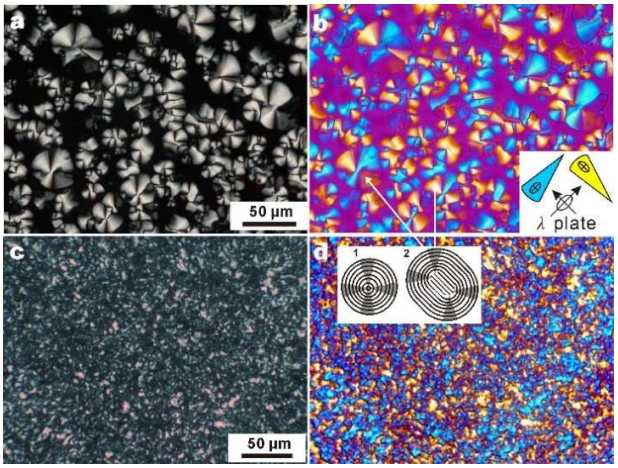

Figure 3. POM textures of (a, b) **2Na** at 93 °C and (c, d) Na salt of 3,4,5-tris-dodecyloxybenzoic acid (**12Na)** at 100 ºC. (b, d) are recorded with a full-wave (λ) retarder plate. The large ellipse in the inset in (b) shows the indicatrix of the retarder, while the small ellipses are indicatrices in the coloured fans of the sample. Inset 1 in (d) shows schematically the concentric circular column configuration in a developable domain with a single +1 disclination in the centre (not seen in the micrographs), while inset 2 shows the case where the central singularity is split into two remote +½ disclinations, as seen in several places in (a, b).

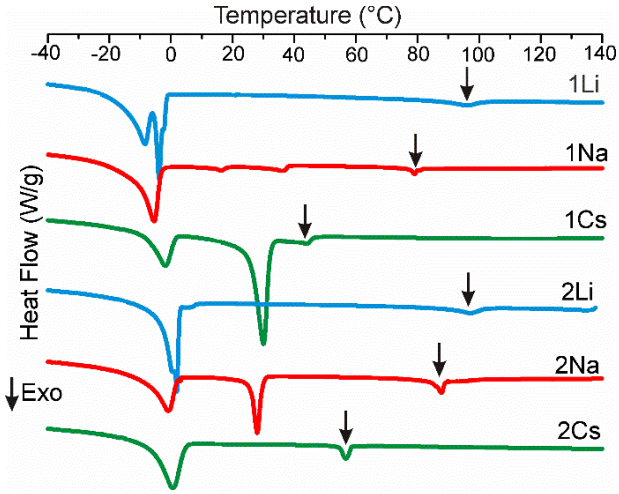

Figure 4**.** DSC thermograms (cooling at 10 K/min) of compounds **1M** and **2M**. The isotropic-columnar transitions are indicated by arrows.

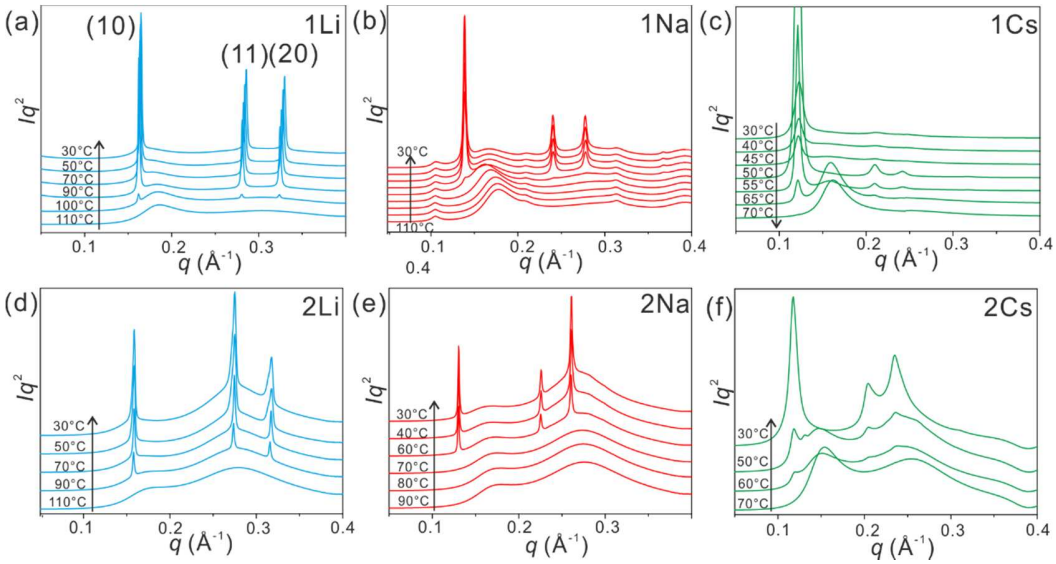

Figure 5. Temperature dependence of transmission powder SAXS curves of compounds **1M** and **2M** recorded at beamline I22 of Diamond Light Source. $q = 4\pi (\sin\theta)/\lambda$, where θ is the Bragg angle and λ the X-ray wavelength. Vertical arrow shows the direction of temperature change.

Temperature dependent powder SAXS curves are shown in Figure 5 and Figures S1-5 in SI. WAXS patterns were recorded simultaneously with SAXS, as shown in Figures S1-5. This ensured that LC phases (mesophases) are clearly distinguished from crystal phases. The nature of the mesophase as hexagonal columnar is confirmed in all six compounds by the presence of three Bragg peaks with the reciprocal square spacings d^{-2} in the ratio 1:3:4; the peaks are thus indexed as (10), (11) and (20) of a hexagonal lattice. For all compounds the appearance of the Bragg peaks on cooling closely matches the temperature of the small sharp exotherm in Figure 4, confirming its assignment as Iso-Col transition.

To confirm the indexing and find out about column orientation and other features, grazing incidence X-ray diffraction experiments were carried out on **1M**

compounds in the form of thin films on silicon substrate – see Figures 6, S2c and 4e. The GISAXS pattern in Figure 6f shows (10), (11) and (20) reflections from **2Na**, sharp both radially and azimuthally, superimposed on semicircles coming from unoriented areas, possibly at sample edges. The diffraction spots come from domains of planar alignment (columns parallel to substrate), but with random in-plane orientation – see model in Figure 5d and the reciprocal space representation of {10} reflections in Figure 6b. We note that reflections from homeotropic areas would be on the equator, but due to the diffraction geometry, these are hidden behind the horizon. In the well-aligned planar domains giving rise to the sharp Bragg spots, the columnar lattice lies on one of its {100} planes, and the same is true for **1Cs** (Figure 6g). However, compared to those of **2Na**, the reflections from **1Cs** are radially considerably broader indicating lattice distortion and/or smaller ordered domains. The significant broadening of reflections in **1Cs** and particularly **2Cs** is also evident from powder SAXS in Figure 5c,f. Notably T_i values of these two compounds are the lowest (Figure 4), suggesting a less stable frustrated structure of the two Cs salts compared with those of Li and Na – see Discussion.

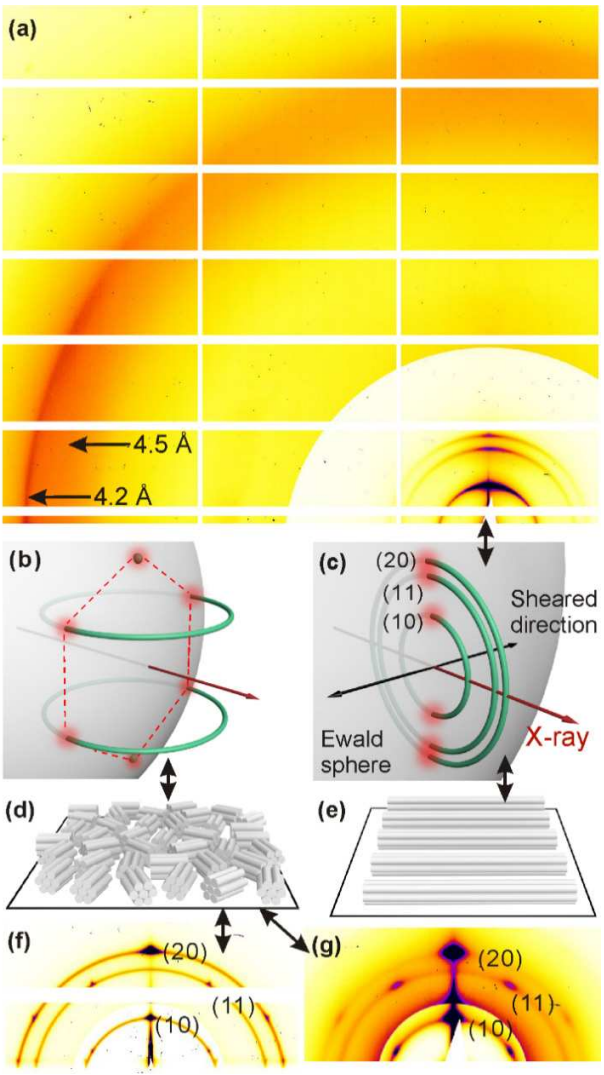

Figure 6. (a) GISAXS/GIWAXS pattern of **1Li** sheared at 120°C and quenched to the columnar phase. The shear direction and the columns are in the horizontal

plane and perpendicular to the beam, as sketched in panel (e). (f) GISAXS of **2Na** at 60°C (cooled from Iso phase); (g) GISAXS of **1Cs** at 45 °C. Columnar domains, randomized in the plane of the substrate, that give the diffraction patterns in (f) and (g) are depicted in (d). The reciprocal space description of diffraction geometry in pattern (a) is given in (e), and that of patterns in (f) and (g) is given in (b). The intersections of the reciprocal rings with the Ewald sphere, giving rise to the diffraction spots (or arcs), are highlighted in red. All experiments were performed at beamline I16 of Diamond Light Source, with thin LC films on Si substrate. The outer region in (a), (f) and (g) is enhanced in intensity. The horizontal and vertical white stripes are gaps between detector panels.

Table 1. Phase transition temperatures, lattice parameters and number of molecules in per unit cell of **1M** and **2M**

Compound	*T*/ °C [ΔH/J g^{-1}]	Lattice parameters		Number of molecules μ^a
		a (Å)	*c* (Å)	
1Li	↓ Iso 96 [2.9] Col -3.9 [7.6] Cr_1 -8.6 [8.5] Cr_2 ↑ -2.3 [8.7] Cr_1 4.9 [7.3] Col 110 [3.5] Iso	44.0	4.2[b]	3.0
1Na	↓ Iso 79 [1.5] Col 36 [1.6] Cr_1 16 [0.5] Cr_2 -5.6 [20] Cr_3 ↑ 2 [22] Cr_2 21 [0.2] Cr_1 42 [0.4] Col 88 [2.2] Iso	52.2	3.7[b]	3.8
1Cs	↓ Iso 44 [1.4] Col 30 [24] Cr_1 -1.8 [8.4] Cr_2 ↑ 2.2 [8.3] Cr_1 49 [17] Col 60/66 [3.7] Iso	59.8	4.5	6.0
2Li	↓ Iso 97 [2.1] Col 1.9 [18] Cr ↑ 5.6 [20] Col 107 [2.9] Iso	46.4	4.0	3.0
2Na	↓ Iso 88 [1.7] Col 28 [7.9] Cr_1 -1.0 [13] Cr_2 ↑ 15 [6.8] Cr_1 41 [7.1] Col 96 [2.6] Iso	55.6	3.7[b]	4.0
2Cs	↓ Iso 57 [1.5] Col 0.3 [18] Cr ↑ 4.3 [18] Col 54/69 [3.2] Iso	61.8	4.5	6.0

[a] See details in SI.
[b] The *d*-spacings observed in GIWAXS.

Figure 6a shows the full grazing incidence diffraction pattern, including the wide-angle region, from a **1Li** film that had been sheared just above T_i in the direction perpendicular to the beam, i.e. left-to-right, and then quenched into the Col phase at 30°C. The fact that all three SAXS peaks are now on the vertical axis means that columns are aligned along the shear direction (Figure 6e) and, moreover, that the orientation of the hexagonal lattice is randomized around the shear direction, rather than the {100} planes lying on the substrate. The geometry in reciprocal space is depicted in Figure 6c. The lack of preferential {100} surface anchoring is attributed to the rapid growth of Col phase on quenching and limited low-temperature mobility hindering the attainment of optimal anchoring. However the shearing experiment has achieved its goal of aligning the columns in a way that condenses the "(001)" reciprocal lattice point in diffraction position on the Ewald sphere (see the arc labelled "4.2 Å" near the horizon in Figure 6a). This scattering maximum is not a true Bragg peak as there is no true long-range order along the column axis. Nevertheless it reflects the average intermolecular distance along the column, allowing the estimation of the volume of the "3-D unit cell" and thus the number of molecules μ in it. The intra-columnar "001" spacings for other compounds were also determined from GIWAXS and these, along with the μ-

values, are listed in Tables 1 and Figure S7. As can be seen, there are 3 molecules per cell in Li salts, 4 in Na salts, and 6 in Cs salts.

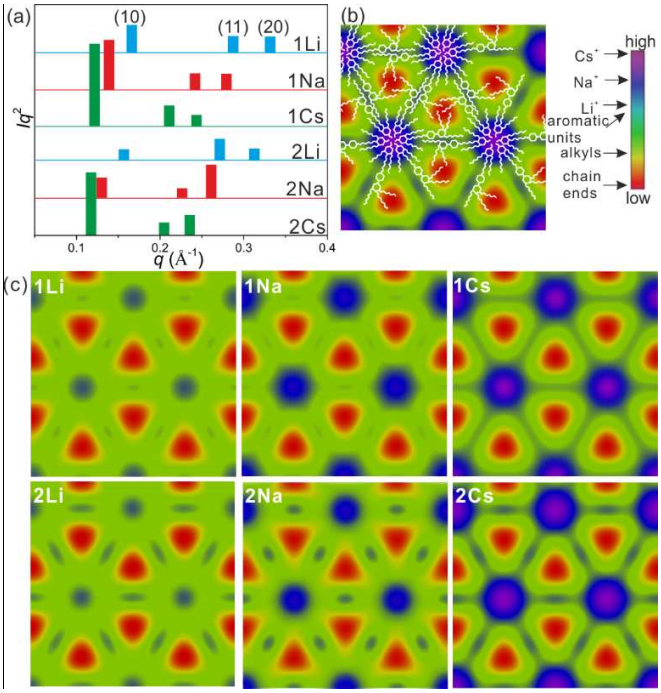

Figure 7. (a) Integrated intensities of the hk Bragg peaks (Lorentz corrected) of the Col_{1+3} phase of compounds **1M** and **2M**. (b) Electron density map of the Col_{1+3} phase of **2Cs** with overlaid schematic molecular model. (c) ED maps of Col_{1+3} phase of all compounds.

In order to determine the molecular arrangement, we first consider the integrated diffraction peak intensities. For easy comparison, these are plotted in Figure 7a. What is unusual is the high intensity of the (11) and (20) peaks, which is normally much lower than that of the (10) peak in most Col phases. This immediately suggests that the structure is not the simple hexagonal arrangement of aromatic columns embedded in an aliphatic continuum. Yet the fact that the relative intensity of the (10) peak increases profoundly with the number of electrons in the metal, i.e. from Li to Cs, suggests that these cations congregate in a single cluster in the unit cell, the site of maximum amplitude of the first term of the Fourier representation of electron density (ED). The full ED maps reconstructed from the powder diffraction intensities in Figure 6a indeed confirm this, as shown in Figure 7b,c. The species most likely to be found in areas of a particular colour are indicated on the colour scale in panel b. Thus the metal-containing columns are found to be arranged on a hexagonal lattice, one per unit cell, with the lowest ED level (blue) in the maps of **1Li** and **2Li**, and the highest (purple) in those of **1Cs** and **2Cs**. The green continuum represent the alkyl chains, which make up 84.7% and 80.2% of the volume of compounds **1M** and **2M**, respectively. The interesting features are the small blobs of elevated ED half way between the main ionic columns. They are more pronounced in **2M** than in **1M** compounds. As shown in the schematic model of the molecular arrangement of **2Cs** in panel (b), these are the locations of the “outer” benzene rings, one per molecule in compounds **1M** and two in compounds **2M**. Not unexpectedly, the points furthest away from benzene rings, i.e. the points where alkyl chains must

stretch to reach, have the lowest density, as shown by the red triangles. Since the unit cell contains 1 major and 3 minor columns, henceforth we denote this phase as Col_{1+3}.

To test the viability of our structures we have built molecular models of each compound on a hexagonal lattice with experimentally determined lattice parameters *a* and *c*, and the number of molecules μ. These were subjected to 30 cycles of molecular dynamics annealing between 300 and 600 K using the Forcite module of Materials Studio (Accelrys). Snapshots of annealed geometry are shown in Figure 8 for **2Li**, **12-12-12Cs**, **1Cs** and **2Cs** (see also Figure S6 for **1Li**). **12-12-12Cs** is the simple single-tapered Cs 3,4,5-*tris*-dodecyloxybenzoate minidendron, reported previously[53] and shown here for comparison (see Discussion). As can be seen, efficient space-filling is achieved in all cases. In compounds **1M** and **2M** the spacer chains, coloured green, are just about long enough in their all-*trans* conformation for the outer benzene rings from neighbouring columns to aggregate together forming separate minor non-ionic aromatic columns half way between the major ionic columns.

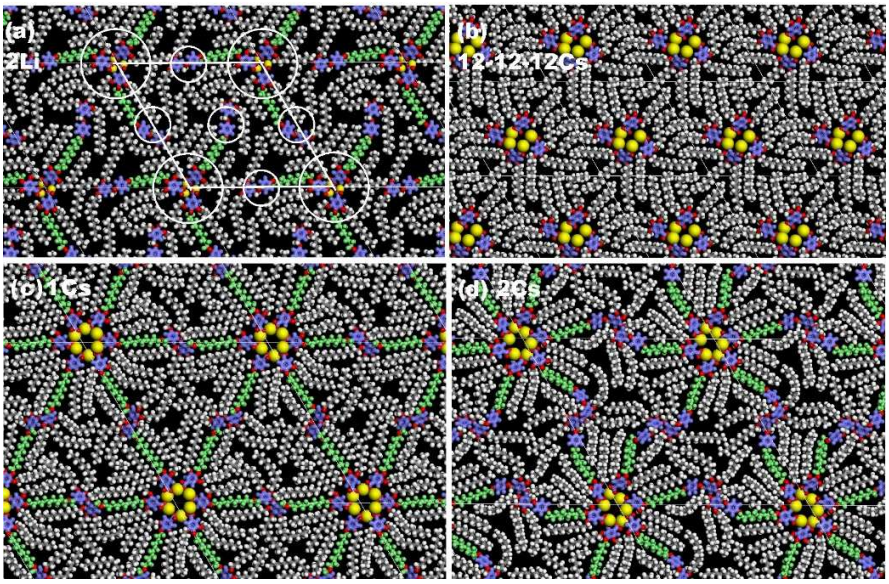

Figure 8. Snapshots of molecular models of compounds (a) **2Li**, (b) **12-12-12Cs**, (c) **1Cs** and (d) **2Cs** after NVT molecular dynamics heat-cool annealing cycles with a total duration of 30 ps. For clarity benzoate and benzylylether groups are purple, cations are yellow, and the linker chains are green. All atoms are ball-and-stick except cations which are CPK with true ionic radii. The unit cell as well as the major (ionic) and minor (non-ionic) columns are indicated in (a).

Since in **1Li** and **2Li** there are only 3 molecules assembling around an ionic column, there can be only one benzene ring, on average, in the cross-section of each of the 6 surrounding minor non-polar columns in **1Li**, and two in **2Li**; these are attached alternatingly to the reference ionic column and to three of the six neighbouring ones. Except in **1Li**, the non-ionic columns are clearly discernible as distinct ED maxima in the maps in Figure 7, and with an intensity consistent with the model, i.e. increasing from Li to Cs, and from **1M** to **2M**. As there are six molecules of **1Cs** and **2Cs** in a cell there are, respectively, 2 and 4 benzene rings in each non-ionic column, half of them attached to the central ionic column and half

to its six ionic neighbours. In the case of **1Na** and **2Na** μ = 4 in an ionic column, hence there must be 4/3 benzene rings, on average, in each minor column in **1Na**, and 8/3 in that of **2Na**. Since the system preserves hexagonal symmetry, non-ionic column strata with 1 and 2 rings in **1Na,** and 2 and 3 rings in **2Na,** must be distributed randomly in the ratio 2:1 and 1:2, respectively.

Discussion

The above results show how redesigning tapered mesogens in a relatively simple way can lead to a novel and complex type of self-assembled "columnar alloy". Learning from these results should help obtain other new complex 2D and, possibly also 3D mesostructures. Keeping within 2D, in principle it is possible to vary the chemical nature of the focal points of the inner and outer fan, one forming e.g. a *p*-semiconducting and the other a *n*-semiconducting π-stacked column type. This would result in a self-assembled columnar mini bulk heterojunction. Similarly, one could construct a complex array comprising ionically and electronically conducting nanowires.

Regarding self-assembly of compounds **1M** and **2M**, there are several further features worth commenting on. First we note the remarkable effect of the size of the alkali metal cation. As the ionic radius increases by no more than 1 Å between Li^+ and Cs^+, and as the benzoate groups are pushed away from the column centre by that small amount, the number of molecules that can fit around the cationic core doubles from 3 to 6, doubling the area of the unit cell. This amplification effect of small differences in the focal group of tapered mesogens can be compared with the similarly striking effect of "bluntness" of the tip of the wedge described in Figure 1.

Another notable difference between the behaviour of single and double-tapered minidendrons is the fact that while in the former the column area decreases steeply with increasing temperature due to widening taper angle and consequent ejection of surplus molecules from the column,[43,46,54,55] in the current double-taper compounds the cell area remains constant (Figure 5). It has been found previously that in the simple single-tapered Li 3,4,5-*tris*-dodecyloxybenzoate minidendron (**12-12-12Li**) there are also, as in **1Li** and **2Li**, only μ = 3 molecules in a column stratum.[53,55] The MD-annealed model of **12-12-12Li** is shown in Figure S6 alongside that of **1Li** for easy comparison. In fact **12-12-12Li** is the only **12-12-12M** salt whose columns do not thin down on heating, as the loss of one of its three molecules in a disk would create an unsustainable void. It was shown, however, that the void could be easily filled, and thus column thinning enabled, if free alkane is added to the minidendron.[53] As in **1Na** and **2Na**, in the simple **12-12-12Na** compound μ = 4 above the crystal melting point. But on further heating there is an unusual first-order Col_{hex}-Col_{hex} phase transition with an abrupt drop in column diameter, due to a cooperative ejection of the fourth minidendron.[55]

As in most other single-taper dendrons, in **12-12-12Cs** column diameter was found to decrease significantly but continuously on heating.[54] At 100 °C $\mu \approx 4$, compared to μ = 6 in **1Cs** and **2Cs**. The MD annealed model of **12-12-12Cs** is shown in Figure 8b. It can be seen that, as adjacent columns in **12-12-12Cs** are closer together than in **1Cs** or **2Cs**, there is more interdigitation of alkyl chains effectively increasing the taper angle of the molecules. In contrast, the exclusion of the outer fans from the inner column corona in **1Cs** and **2Cs** increases the distance between the ionic columns to the point where intercolumnar interdigitation ceases to be an option. Some interdigitation does occur, but this is between the

chains of the major and the minor columns. As most of the chains of the outer fans are now engaged in filling the depleted interstitial zones (red triangles in Figure 7b, c), the degree of interdigitation is considerably reduced. This reduces the effective taper angle of the inner fans, allowing μ of **1Cs** and **2Cs** to increase from ~4 to 6, and staying at 6 up to the clearing temperature. The same reasoning explains why in double-tapered Na salts μ is constant at 4, while in **12-12-12Na** it decreases sharply from 4 to nearly 3 on heating.[55]

From the low T_i (Figure 4) and poor order in the Col_{1+3} phase of **1Cs** and **2Cs** (broad Bragg peaks in Figure 5c, f) it is clear that the Col_{1+3} structure in double-tapered Cs minidendrons is a highly frustrated one, compared to those in Li and Na compounds. We attribute this to the low conformational entropy of this structure, with only a low *gauche/trans* ratio allowed by the need to keep the outer fans outside the inner column shell of exceptionally large diameter.

In this context we also comment on the shape of the SAXS curves of the Iso liquid above T_i **(**Figure 5, bottom curves in all panels**)**. Normally above the clearing temperature of a columnar LC a diffuse scattering maximum remains close to the position of the (10) Bragg peak of the Col phase; this reflects the persistence of short-range columnar order in the Iso liquid. However in the present compounds there are two diffuse maxima in the Iso phase, the second one particularly pronounced in **2M** compounds. The *q*-values of the two peaks are roughly in the ratio 1:$\sqrt{3}$, suggesting short-range hexagonal order. The first peak intensifies in the order of cations Li^+ - Na^+ - Cs^+, indicating that it is dominated by the correlation between persisting ionic columns. The peak is clearly shifted to higher *q* away from that of the (10) Bragg peak, particularly in Na and Cs compounds. This suggests that, upon isotropization, the column diameter shrinks substantially, but only after the steric constraints of the Col_{1+3} phase had been relaxed. In fact in the Iso phase of all six compounds the first maximum is almost at the same position of 0.17 $\pm$ 0.1 $Å^{-1}$, which corresponds to a spacing of $2\pi/q \approx 37$ Å. This would suggest a significant reduction in the number of dendrons per column, probably to no more than 3, upon Col_{1+3}-Iso transition. It is also notable that the second diffuse peak is much stronger in **2M** than in **1M** compounds, reflecting correlation between all columns, non-ionic as well as ionic, with the additional benzene ring in **2M** making the two column types more similar in electron numbers. However, the persistence of the low-*q* peak in the Iso phase of all compounds confirms that fragments of the basic Col_{1+3} pattern remain in the Iso liquid.

The fact that the second diffuse Iso peak, the "$(11)_{Iso}$", coincides with the (20) Bragg peak of the Col_{1+3} phase in **2Na** and **2Cs** can be represented schematically as in Figure 9a. The relationship between the two arrays, the Col_{1+3} (black) and the Iso "lattice" (red) is obtained by rotating the unit cell by 30°, whereby the distance between the major (ionic) and minor (non-ionic) columns drops from d_{11} to d_{20}, i.e. by a factor $\sqrt{3}/2$. However, in spite of the unit cell shrinking, the inter-chain distance increases on isotropization, as indicated by the shift to lower *q* of the diffuse WAXS peak (Figure S5b).

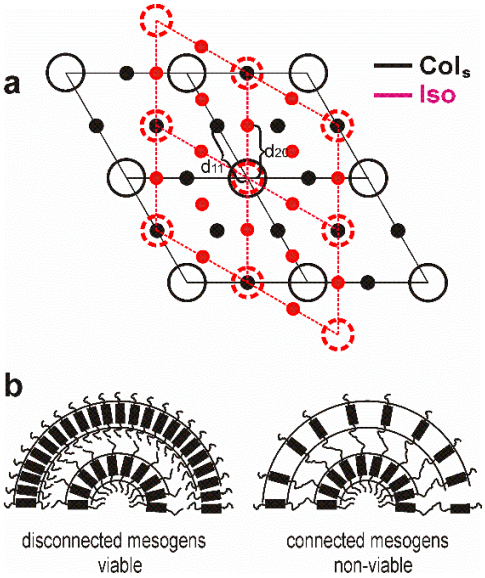

Figure 9. (a) Schematic model showing the relationship between the 1+3 type columnar arrangements in the Col (black) and Iso (red) phases. Empty circles are ionic and small full circles non-ionic columns. The arrangement in Iso phase is only short-range. Four unit cells are shown for each structure. d_{11} and d_{20} are lattice spacings in the Col phase. (b) Qualitative explanation of the high bending modulus of covalently linked columns in the "topologically stiff" Col_{1+3} phase (right), compared to the low modulus of non-linked columns in an ordinary Col phase (left). The black rectangles represent discotic molecules or supramolecular self-assembled discs.

Finally a comment on the optical textures. In areas of planar alignment Col_{1+3} phase of compounds **1M** and **2M** grows large developable domains with fan-like appearance (Figure 3a,b). These are very different from the fine and irregular textures displayed by most single taper minidendrons (Figure 3c,d and ref. [56]). Even where larger domains were observed in single-taper compounds, most were marked by a clear central disclination of strength s = +1, evidenced by a Maltese cross with four dark brushes meeting in the centre, as depicted in Inset 1 in Figure 3d.[57] Such textures are indicative of a low bending modulus (low Frank constant K_3),[58] as is expected from highly flexible columns containing a high aliphatic fraction and no large rigid mesogens. However, in the "spherulites" of compounds **1M** and **2M**, the central disclination is always split in two clearly separated s = +1/2 disclinations – see Figure 2a,b and Inset 2 in panel d. This means that the columns are stiff (high K_3) and cannot withstand high curvature. So what is the origin of the stiffness of the Col_{1+3} phase, of which 80-85% consists of molten alkyl chains and the rest are flexibly connected single benzene rings?

We explain this puzzling observation with the help of the sketch in Figure 9b. The figure on the left shows half of the centre of a +1 disclination in the Col phase of single-tapered mesogens or of an ordinary small discotic mesogen. Such columns can be highly bendable, and circles of radius r down to the size of a single molecule have been observed by high-resolution atomic force microscopy.[59] But in the case of Col_{1+3} where neighbouring columns, in this case the major and minor columns, are connected by covalent linkers, the outer circle with larger circumference is still restricted to containing the same number of mesogens as the inner circle. Consequently the relative distortion in intermolecular spacing in two

successive circular columns is $\Delta c/c = d/r$, where d is the width of the column. Only for sufficiently large r will the relative distortion be small enough for the cumulative energy of all distortions along the innermost loop of the s = ½ disclination to drop below the end energy of the bundle of straight but truncated columns in the middle (Inset 2 of Figure 3d).

This origin of column stiffness is distinct from the usual case of inflexible columns of large discotic mesogens, and it can be regarded as topological in nature; the Col_{1+3} structure can thus be regarded as "topologically stiff". One can draw a parallel with a similarly topological nature of high splay elastic constant K_1 in main-chain nematic polymers, which is primarily due not to the intrinsic rigidity of the chains, but to the scarcity of chain ends needed for insertion between diverging chains.[60]

Conclusion

We have synthesised the first examples of double-tapered mesogens and obtained a new type of hexagonal columnar LC superlattice consisting of two kinds of columns, major and minor, in the ratio 1:3. The double-tapered anionic minidendrons are held together by Li, Na or Cs cations, the size of which strongly affects the number of molecules in the unit cell. Optical textures indicate surprisingly high columnar bending modulus, attributed here to topological resistance to curvature. Based on the structural model presented, we can propose ways to increase the stability of specific structures; e.g. an increase in linker length will further stabilize the Col_{1+3} phase of Cs compounds. The coexistence of ionic and non-ionic columns in an ordered superlattice points the way to creating novel materials with double functionality. Moreover, unlike other columnar LCs, this structure has zero lateral thermal expansivity, which is highly desirable in nanopatterning applications. We note that high dimensional stability has recently also been achieved in a honeycomb-type columnar LC, but this was based on a framework of in-plane lying rigid rod-like mesogens.[61] The present work is expected to lead to the design of further novel complex 2D columnar and 3D micellar soft alloy-like mesophases.

Acknowledgements

This work was supported by the National Natural Science Foundation of China, Grants 21772178 and 21674099, by EPSRC (UK), grant EP_P002250, and by CNCS - UEFISCDI (Romania), project PN-III-P4-ID-PCE-20160720 within PNCDI-III. YL thanks CSC for stipend and University of Sheffield for waiving tuition fees. For help with synchrotron experiments we thank Prof. N. Terrill and Dr. O. Shebanova, beamline I22, and Dr. Gareth Nisbet, beamline I16 at Diamond Light Source.

[1] S. Chandrasekhar, B. K. Sadashiva, K. A. Suresh, *Pramana* **1977**, *9*, 471–480.
[2] F. Vera, J. L. Serrano, T. Sierra, *Chem. Soc. Rev*. **2009**, *38* 781-796.
[3] H. Detert, M. Lehmann, H. Meier, *Materials* **2010,** *3*, 3218-3330.
[4] K. V. Le, H. Takezoe, F. Araoka, Adv. Mater. **2017**, *29*, 1602737.
[5] Malthéte, J.; Collet, A. *J. Am. Chem. Soc.* **1987**, *109*, 7544-7545.

[6] C. Roche, H.-J. Sun, M. Prendergast, P. Leowanawat, B. Partridge, P. A. Heiney, F. Araoka, R. Graf, H. W. Spiess, X.B. Zeng, G. Ungar, V. Percec *J. Am. Chem. Soc.* **2014**, 136, 7169–7185.
[7] M. A. Shcherbina, X.Zeng, T. Tadjiev, G.Ungar, S.H.Eichhorn, K. E. S.Phillips, T.J. Katz, *Angew. Chem. Int. Ed.,* **2009**, *48*, 7837-7840.
[8] T. Ghosh, M. Lehmann, *J. Mater. Chem. C* **2017**, *5*, 12308-12337
[9] C. Tschierske, C. Nürnberger, H. Ebert, B. Glettner, M. Prehm, F. Liu, X. B. Zeng and G. Ungar, *Interface Focus*, **2012**, *2*, 669–680.
[10] J. Barbera, L. Puig, P. RomeroJ. L. Serrano, T. Sierra, *J. Am. Chem. Soc*. **2006**, *128,* 4487–4492.
[11] A. Das, S. Ghosh, *Angew. Chem. Int. Ed.* **2014**, *53*, 2038 – 2054.
[12] Tanabe, K.; Suzui, Y.; Hasegawa, M.; Kato, T. *J. Am. Chem. Soc.* **2012**, *134,* 5652–5661.
[13] F. Morale, R. L. Finn, S. R. Collinson, A. J. Blake, C. Wilson, D. W. Bruce, D. Guillon, B. Donnio, M. Schroder, *New J. Chem.* **2008**, *32*, 297-305.
[14] B. M. Rosen, C. J. Wilson, D. A. Wilson, M. Peterca, M. R. Imam, V. Percec, *Chem. Rev.* **2009**, *109*, 6275-6540.
[15] S. Hecht, J. M. Frechet, *Angew. Chem. Int. Ed*. **2001**, *40*, 74–91.
[16] B. Donnio, S. Buathong, I. Bury, D. Guillon, *Chem. Soc. Rev*. **2007**, *36*, 1495–1513.
[17] C. Tschierske, *Angew. Chem. Int. Ed*. **2013**, *52*, 8828-8878.
[18] T. Kato, N. Mizoshita, K. Kishimoto, *Angew. Chem., Int. Ed*. **2006**, *45*, 38–68.
[19] H. J. Sun, S. D. Zhang, V. Percec, *Chem. Soc. Rev.* **2015**, *44*, 3900-3923.
[20] F. Würthner, C. Thalacker, S. Diele, C. Tschierske, *Chem. Eur. J.* **2001,** *7*, 2245-2253.
[21] Z. Z. An, J. S. Yu, B. Domercq, S. C. Jones, S. Barlow, B. Kippelen, S. R. Marder, *J. Mater. Chem.* **2009**, *19*, 6688-6698.
[22] G. Ungar, S.V. Batty, V. Percec, J. Heck, G. Johansson, *Adv. Mater. Opt. Electro*. **1994**, *4*, 303–313.
[23] T. Ichikawa, M. Yoshio, A. Hamasaki, T. Mukai, H. Ohno, T. Kato, *J. Am. Chem. Soc.* **2007**, *129*, 10662–10663.
[24] M. Peterca, V. Percec, A. E. Dulcey, S. Nummelin, S. Korey, M. Ilies, P. A. Heiney, *J. Am. Chem. Soc.* **2006**, *128*, 6713–6720.
[25] C. S. Pecinovsky, E. S. Hatakeyama, D. L. Gin, *Adv. Mater.* **2008**, *20*, 174–178.
[26] B. Soberats, M. Yoshio, T. Ichikawa, X. B. Zeng, S. Taguchi, H. Ohno, F. Liu, G. Ungar, T. Kato, *J. Am. Chem. Soc.* **2015**, *137*, 13212-13215.
[27] G. Johansson, V. Percec, G. Ungar, D. Abramic, *J. Chem. Soc., Perkin Trans. 1* **1994**, 447-459.
[28] A. Schultz, S. Laschat, A. Saipa, F. Gießelmann, M. Nimtz, J. L. Schulte, A. Baro, B. Miehlich, *Adv. Funct. Mater.* **2004**, *14*, 163-168.
[29] V. Percec, M. Glodde, T. K. Bera, Y. Miura, I. Shiyanovskaya, K. D. Singer, V. S. K. Balagurusamy, P. A. Heiney, I. Schnell, A. Rapp, H.-W. Spiess, S. D. Hudson, H. Duan, *Nature* **2002**, *419*, 384-387.
[30] T. T. Steckler, X. Zhang, J. Hwang, R. Honeyager, S. Ohira, X. H. Zhang, A. Grant, S. Ellinger, S. A. Odom, D. Sweat, D. B. Tanner, A. G. Rinzler, S. Barlow, J. L. Bredas, B. Kippelen, S. R. Marder, J. R. Reynolds, *J. Am. Chem. Soc.* **2009**, *131*, 2824-2826.
[31] D. J. P. Yeardley, G. Ungar, V. Percec, N. M. Holerca, G. Johansson, *J. Am. Chem. Soc.* **2000**, *122*, 1684-1689.

[32] Y. Tsuda, R. Kuwahara, J. -M. Oh, *Trans. Mater. Res. Soc. Jpn.* **2004**, *29*, 267-271.
[33] A. Grotzky, E. Atamura, J. Adamcik, P. Carrara, P. Stano, F. Mavelli, T. Nauser, R. Mezzenga, A. D. Schluter, *Langmuir* **2013**, *29,* 10831-10840.
[34] V. Percec, A. E. Dulcey, M. Peterca, P. Adelman, R. Samant, V. S. K. Balagurusamy, P. A. Heiney, *J. Am. Chem. Soc.* **2007**, *129*, 5992-6002.
[35] B. Donnio, P. Garcia-Vazquez, J. -L. Gallani, D. Guillon, E. Terazzi, *Adv. Mater*. **2007**, *19*, 3534-3539.
[36] K. Kanie, M. Matsubara, X. B. Zeng, F. Liu, G. Ungar, H. Nakamura, A. Muramatsu, *J. Am. Chem. Soc*. **2012**, *134*, 808-811.
[37] X. Feng, M. E. Tousley, M. G. Cowan, B. R. Wiesenauer, S. Nejati, Y. Choo, R. D. Noble, M. Elimelech, D. L. Gin, C. O. Osuji, *ACS Nano* **2014**, *8*, 11977–11986.
[38] S. Zhang, H. -J. Sun, A. D. Hughes, R. O. Moussodia, A. Bertin, Y. Chen, D. J. Pochan, P. A. Heiney, M. L. Klein, V. Percec, *Proc. Natl. Acad. Sci. U. S. A.* **2014**, *111*, 9058–9063.
[39] B. P. Hoag, D. L. Gin, *Liq. Cryst.* **2004**, *31*, 185-199.
[40] G. Ungar, F. Liu, X. B. Zeng, *Handbook of Liquid Crystals***,** Vol. 5(Eds.: J. W. Goodby, P. J. Collings, T. Kato, C. Tschierske, H. F. Gleeson, P. Raynes), VCH_Wiley, Weinheim, 2nd Ed., **2014**, pp. 363-436.
[41] D. R. Dukeson, G. Ungar, V. S. K. Balagurusamy, V. Percec, G. Johansson, M. Glodde, *J. Am. Chem. Soc.* **2003**, *125*, 15974-15980.
[42] D. J. P. Yeardley, G. Ungar, V. Percec, N. M. Holerca, G. Johansson, *J. Am. Chem. Soc*., **2000**, *122*, 1684-1689.
[43] X. H. Yao, L. Cseh, X. B. Zeng, M. Xue, Y. S. Liu, G. Ungar, *Nanoscale Horiz.* **2017**, *2*, 43-49.
[44] A. C. Ribeiro, B. Heinrich, C. Cruz, H. T. Nguyen, S. Diele, M. W. Schroeder, D. Guillon, *Eur. Phys. J. E* **2003**, *10*, 143–151.
[45] V. Percec, C. M. Mitchell, W. -D. Cho, S. Uchida, M. Glodde, G. Ungar, X. B. Zeng, Y. Liu, V. S. K. Balagurusamy, P. A. Heiney, *J. Am. Chem. Soc*. **2004**, *126,* 6078-6094.
[46] V. Percec, M. N. Holerca, S. Uchida, W. D. Cho, G. Ungar, Y. S. Liu, D. J. P. Yeardley, *Chem. Eur. J*. **2002**, *8*, 1106-1117.
[47] T. Woehrle, I. Wurzbach, J. Kirres, A. Kostidou, N. Kapernaum, J. Litterscheidt, J. C. Haenle, P. Staffeld, A. Baro, F. Giesselmann, S. Laschat, *Chem. Rev.* **2016**, *116*, 1139−1241.
[48] G. Ungar, D. Abramic, V. Percec, J. Heck, *Liq. Cryst.* **1996**, *21*, 73-86.
[49] M. A. Shcherbina, X. B. Zeng, T. Tadjiev, G. Ungar, S. H. Eichhorn, K. E. S. Phillips, T. J. Katz, *Angew. Chem. Int. Ed.* **2009**, *48*, 7837-7840.
[50] B. M. Rosen, D. A. Wilson, C. J. Wilson, M. Peterca, B. C. Won, C. -H. Huang, L. R. Lipski, X. B. Zeng, G. Ungar, P. A. Heiney, V. Percec, *J. Am. Chem. Soc.* **2009**, *131*, 17500–17521.
[51] M. Peterca, M. R. Imam, P. Leowanawat, B. M. Rosen, D. A. Wilson, C. J. Wilson, X. B. Zeng, G. Ungar, P. A. Heiney, V. Percec, *J. Am. Chem. Soc.* **2010**, *132*, 11288–11305.
[52] M. Kleman, *J. Physique* **1980**, *41*, 737-745.
[53] M.-H. Yen, J. Chaiprapa, X. B. Zeng, Y. Liu, L. Cseh, G. H. Mehl, G. Ungar, *J. Am. Chem. Soc.* **2016**, *138*, 5757–5760.
[54] G. Ungar, V. Percec, M. N. Holerca, G. Johansson, J. A. Heck, *Chem. Eur. J.* **2000**, *6*, 1258-1266.

[55] W. S. Fall, M. H. Yen, X. B. Zeng, L. Cseh, Y. S. Liu, G. A. Gehring, G. Ungar, *Soft Matter* **2019**, *15*, 22 – 29.
[56] X. Feng, S. Nejati, M. G. Cowan, M. E. Tousley, B. R. Wiesenauer, R. D. Noble, M. Elimelech, D. L. Gin, C. O. Osuji, *ACS Nano* **2016**, *10*, 150−158.
[57] U. Beginn, L. Yan, S. N. Chvalun, M. Shcherbina, A. V. Bakirov, M. Möller, *Liq. Cryst.* **2008**, *35*, 1073–1093.
[58] P. G. de Gennes, J. Prost, *Physics of Liquid Crystals.* 2nd Ed., Clarendon Press, Oxford, **1993**, pp: 98-155.
[59] (a) R. B. Zhang, X. B. Zeng, B. -S. Kim, R. Bushby, K. -S. Shin, P. Baker, V. Percec, G. Ungar, *ACS Nano*. **2015**, *9*, 1759-1766; (b) R. B. Zhang, X. B. Zeng, C. Y. Wu, Q. Jin, Y. S. Liu, G. Ungar, *Adv. Funct. Mater*. **2019**, *29*, 1806078, Doi: 10.1002/adfm.201806078.
[60] A. Popadić, D. Svenšek, R. Podgornik, K. C. Daoulas, M. Praprotnik, *Soft Matter.* **2018**,*14*, 5898-5905.
[61] W. S. Fall, C. Nürnberger, X.B. Zeng, F. Liu, S. J. Kearney, G. A. Gehring, C. Tschierske, G. Ungar, *Mol. Syst. Des. Eng*. **2019**, *4*, 396-406.

Table of Contents Entry

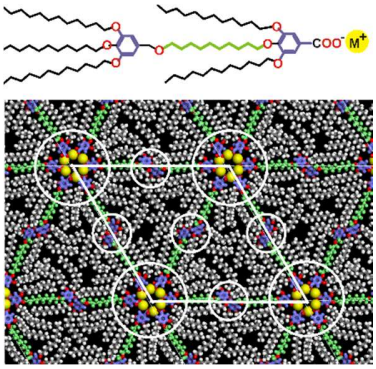

Introduction of double-taper shaped molecules using a series of simple model carboxylate salt minidendrons opens a route to complex self-assembly of mixed columns, mixed spheres, or mixed columns and spheres, leading potentially to new self-organized multifunctional materials.

Keywords:

Dendrimers
GISAXS
Liquid crystals
Self-assembly
X-ray diffraction